



HAL
open science

Radar Cross-Section Pattern Measurement of a Complex Target in Reverberation Chamber

C. Charlo, S. Méric, F. Sarrazin, J. Sol, P Pouliguen, Elodie Richalot, P. Besnier

► **To cite this version:**

C. Charlo, S. Méric, F. Sarrazin, J. Sol, P Pouliguen, et al.. Radar Cross-Section Pattern Measurement of a Complex Target in Reverberation Chamber. 20th European Radar Conference, EuRAD 2023, Sep 2023, Berlin, Germany. pp.22-25, 10.23919/EuRAD58043.2023.10289341 . hal-04337820

HAL Id: hal-04337820

<https://hal.science/hal-04337820v1>

Submitted on 11 Nov 2024

HAL is a multi-disciplinary open access archive for the deposit and dissemination of scientific research documents, whether they are published or not. The documents may come from teaching and research institutions in France or abroad, or from public or private research centers.

L'archive ouverte pluridisciplinaire **HAL**, est destinée au dépôt et à la diffusion de documents scientifiques de niveau recherche, publiés ou non, émanant des établissements d'enseignement et de recherche français ou étrangers, des laboratoires publics ou privés.

Radar Cross-Section Pattern Measurement of a Complex Target in Reverberation Chamber

C. Charlo^{#1}, S. Méric^{#2}, F. Sarrazin^{#3}, J. Sol[#], P. Pouliguen⁺, E. Richalot^{*}, P. Besnier^{#4},

[#]Univ Rennes, INSA Rennes, CNRS, IETR-UMR 6164, F-35000 Rennes, France

^{*}Univ Gustave Eiffel, CNRS, ESYCOM, F-77454 Marne-la-Vallée, France

⁺Defense Innovation Agency, French Ministry of Armed Forces, Paris, France

{corentin.charlo^{#1}, stephane.meric^{#2}, philippe.besnier^{#4}}@insa-rennes.fr, francois.sarrazin@univ-rennes.fr^{#3}

philippe.pouliguen@intradef.gouv.fr⁺, elodie.richalot-taisne@univ-eiffel.fr^{*}

Abstract— Radar cross-section (RCS) measurements using reverberation chambers (RCs) have been recently introduced and improved firstly for estimating the most important scattering directions before being able to also retrieve the RCS level. In this communication, this method is extended to the RCS measurement of a complex target. Measurement results in both HH and VV polarizations are shown to be very consistent with simulation results using CST Studio Suite. Furthermore, the distance of the main scattering areas according to the azimuth angle is reported.

Keywords— Radar Cross-Section, Reverberation Chamber, Complex Target, Measurements.

I. INTRODUCTION

The RCS describes the scattering behaviour of an object when it is illuminated by an electromagnetic wave. Nowadays, the RCS of an object is of great interest for a lot of applications. RCS measurements are key to either investigating or reducing the signature of numerous equipment for military applications or to ensure the possible detection of various objects for civil radar sensors. Usually, this type of measurement is performed in an anechoic chamber to extract the line-of-sight contribution of the target while reducing the multipath contributions. However, this type of chamber is expensive and not much available outside academic or military laboratories.

Originally developed for electromagnetic compatibility testings, RCs have extended their applications to various types of characterization as evidenced in early articles and some recent textbooks [1], [2], [3]. Some of their applications concern antenna characterization [4], over the air testing of wireless devices [5], and they can also be used as exposure system for bio-electromagnetic application [6]. In particular, RCS measurement in RCs is now a subject of interest and a few methods have been used to this effect. The method proposed in [7] consists of a post-processing step where a time-gating is applied on the time-domain signal obtained after an inverse Fourier transform calculation; indeed, it corresponds to the classical approach used for RCS measurement in anechoic chamber or any arbitrary test environment. In another article [8], the measurement principle is based on the estimation of the Ricean K-factor [5], that corresponds to the ratio between the scattered field from the device under test and the incoherent

field associated to multiple reflection in the RC. The K -factor is then used to extract the line-of-sight signal between the target and the antennas, and finally, the direct path is used to extract the target RCS. However, this method has a limited RCS dynamic range. In [9], authors propose to exploit the Doppler effect. The target is moved within the RC in the direction of the antennas, generating virtually a Doppler effect on the backscattered signal. This method has a better dynamic but requires a rail to move the target.

In this article, RCS estimations are based on a sinusoidal regression applied to the difference of the S-parameters between the empty room and the charged room [10], [11], [12]. According to a recent improvement of this method, the RCS estimation is performed in two steps [13]. A first step consists in estimating the appropriate distance of the most important scattering zone, whereas the second step allows the identification of the sinusoidal regression amplitude, the RCS of the target being directly proportional to that amplitude.

This manuscript is organised as follows. Section II briefly explains the hypothesis and the principle of RCS measurement in RCs and the two-step method as shown in [10], [11], [12], [13]. Then, the measurement setup and the target are detailed in the section III. In Section IV, the results of the RCS measurement and comparison with CST Studio Suite simulation are shown. The last section concludes.

II. THEORY OF RCS MEASUREMENT IN RCs

The theoretical development of the RCS measurement in RCs can be found in details in [11], [12], [13] and is briefly recalled in this section. The RCS is extracted from the difference of the scattering parameters measured in an empty RC ($S_{xy}(f_0)$) and the RC loaded with the target ($S_{xy}^T(f_0)$). This difference $\Delta S(f_0)$ is expressed in (1) where the azimuth angle variable is omitted for simplification purpose.

$$\Delta S(f_0) = S_{xy}^T(f_0) - S_{xy}(f_0) = B(f_0) + A(f_0) \times \exp\left(-j \frac{2\pi f_0}{\delta f}\right) \times \exp(j\phi_0) \quad (1)$$

with

$$B(f_0) = \sqrt{m_x(f_0)m_y(f_0)} \times \sqrt{\eta_x(f_0)\eta_y(f_0)} \times (H^T(f_0) - H(f_0)) \quad (2)$$

$$A(f_0) = \sqrt{\sigma^T(f_0)} \frac{c\sqrt{m_x(f_0)m_y(f_0)G_x(f_0)G_y(f_0)}}{(4\pi)^{3/2}R'^2 f_0} \quad (3)$$

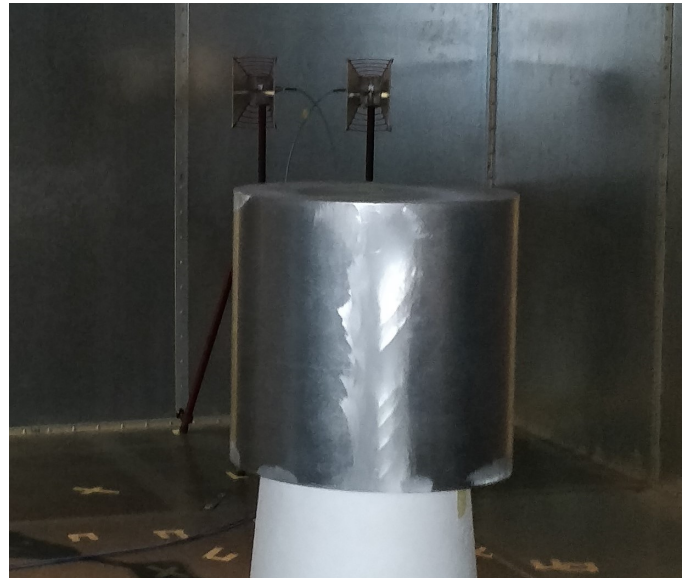
The difference $\Delta S(f_0)$ is written as the addition of two terms. The first term $B(f_0)$ (2) depends on the free-space (FS) antenna mismatching coefficient $m_i(f_0) = 1 - |S_{ii\text{FS}}(f_0)|^2$ with $i = \{x, y\}$, the antenna radiation efficiency $\eta_i(f_0)$ and the difference of the two random variables representing the RC transfer function with the target ($H^T(f_0)$) and without the target ($H(f_0)$). These two variables have the same variance and are distributed according to a centered Gaussian probability density function. The second term $A(f_0) \times \exp(-j\frac{2\pi f_0}{\delta f}) \times \exp(j\phi_0)$ corresponds to the radar echo which is proportional to the square root of the target RCS. In (3), the terms $G_i(f_0)$ with $i = \{x, y\}$ are the gain of the antennas and R' is the physical distance between the target and the antennas. This echo can be approximated as a sinusoidal function around the central frequency f_0 in the frequency domain. The periodicity of this sinusoidal signal $\delta f = c/(2R)$ depends on the electrical distance. Besides, a constant phase ϕ_0 is considered.

Finally, the RCS value $\sigma^T(f_0)$ is computed by the estimation of the amplitude of the difference according to a sinusoid regression. This sinusoid regression is used on two different frequency bandwidths as detailed in [13]. The electrical distance between the antennas and the target is estimated applying the sinusoid regression on the whole 4 GHz frequency bandwidth. Then, using this estimated distance, the amplitude of the difference of the S-parameters is computed on a smaller frequency bandwidth. In this article, the chosen frequency bandwidth is of 0.9 GHz as in [13], as it has been shown to be suited for IETR RC in this frequency range. The RCS measurements are calibrated with the RCS measurement of a metallic plate of $0.152 \times 0.150 \text{ m}^2$ placed at the same location in the RC.

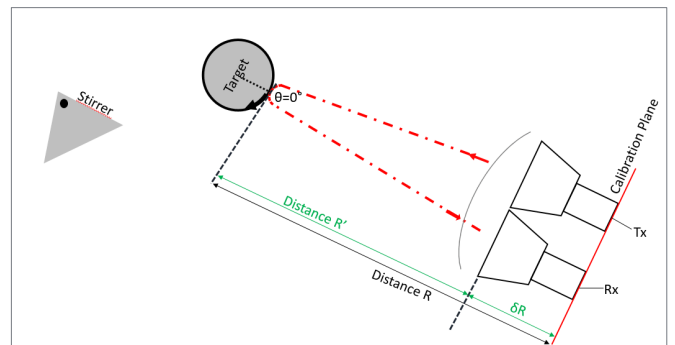
III. MEASUREMENT SETUP

Measurements are made in the largest RC of the IETR laboratory whose dimensions are $2.9 \text{ m} \times 3.7 \text{ m} \times 8.7 \text{ m}$. The quasi-monostatic RCS measurement is realized with two horn antennas (ETS-Lindgren model 3115). The two antennas are close to each other regarding the distance between the antennas and the target, and there are oriented towards the target. It has been verified that the coupling between these two close antennas does not affect the RCS measurement [12]. Antennas are turned to perform measurements in VV then HH polarization.

The measurement setup is described in Fig. 1. The orientation of the antennas-target axis is not perpendicular to any cavity wall in order to avoid any spurious echo from



(a) Picture of the measurement set up in HH polarization in the RC with the back of the target in the foreground and the antennas at the background.



(b) Schematic description with distance definitions

Fig. 1. Picture in HH polarization (a) and schematic description with distance definitions (b) of the test setup with a cylindrical target in the RC.

the wall behind the target. The distance R' between the antennas and the middle of the rotating mast is fixed to 4.6 m. This distance R' is smaller than $\frac{2D^2}{\lambda}$ where D is the largest dimension of the target and λ is the wavelength. This distance has been chosen to respect as much as possible the far-field condition while being limited by the RC size. The target is placed on a rotating mast for characterization. The measurements are performed around the central frequency of 9.2 GHz. The frequency bandwidth is of 4 GHz with a IF filter of 1 kHz and a frequency step of 100 kHz. During its rotation, the azimuth angle of the target varies between -100° and $+100^\circ$ with a rotation step of 1° . As the angle positions are corrected so that the $\theta = 0^\circ$ angle corresponds to a local maximum, the final results are only given in the $\pm 90^\circ$ range.

The target under test is a metallic cylinder with a shallow excavation compared to wavelength, whose schematic is presented in Fig.2. The height of this target is of 30 cm and the radius of this cylinder is of 15 cm. The shallow excavation appears in the middle of the cylinder. The dimension of this

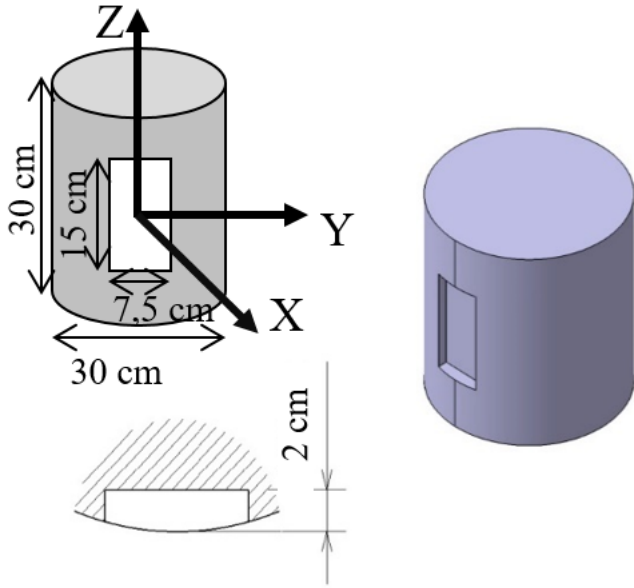


Fig. 2. Description of the measured metallic cylinder with the shallow excavation.

excavation is $15 \text{ cm} \times 7.5 \text{ cm}$ with a depth of 2 cm. This depth is close to the wavelength $\lambda = \frac{c}{f} \approx 3.3 \text{ cm}$.

IV. MEASUREMENT RESULTS

This section presents the RCS pattern measurement results in VV and HH polarizations, and compare them with the simulated ones obtained using a CST Studio Suite simulation as reference.

A. RCS reference using CST Studio Suite

The simulation on CST Studio Suite are made using the RCS module software for a plane wave excitation. It has to be noticed that this plane wave would correspond to a source as a infinite distance, unlike in measurement. The target is considered as made of perfect electric conductor and placed in vacuum. The simulation is performed at 9.2 GHz using the time solver, and the accuracy is fixed to -40 dB . The RCS was computed over an azimuth range between 0° and $+90^\circ$ with a 1° step, and the results between -90° and -1° are obtained according to symmetry considerations. The target symmetry with respect to XY plane is used to increase the simulation accuracy.

B. VV Polarisation

In this section, the target is illuminated in VV polarization. The two-step method is applied to extract the RCS. First, the antenna-target distance estimated on the 4 GHz frequency bandwidth is shown in blue in Fig. 3. This figure highlights the accuracy of the distance estimation as the shallow excavation is well detected with a distance difference between the angles $\theta = -14^\circ$ and $\theta = 14^\circ$ of 2 cm that corresponds to its depth. On the rest of the azimuth range, the estimated distance stays stable. Moreover, this estimated distance is symmetric

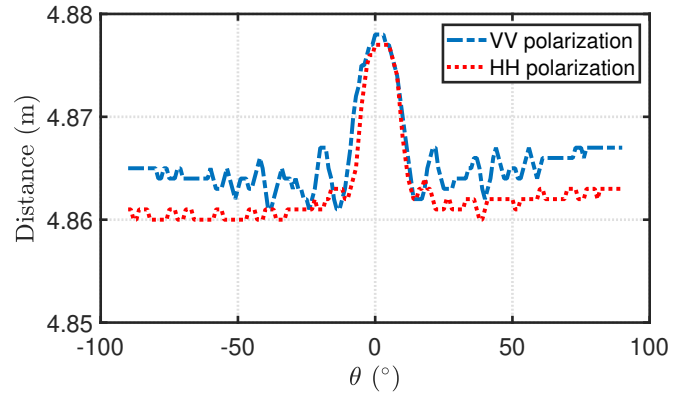


Fig. 3. Estimation of the distance between the target and the antennas as a function of the azimuth angle θ varying from $\theta = -90^\circ$ to $\theta = 90^\circ$ for the two different measurements configurations.

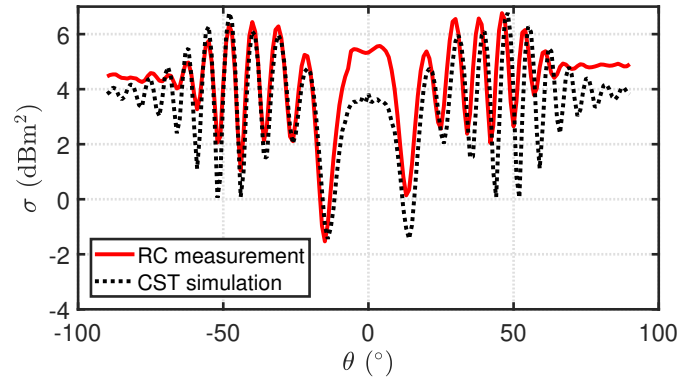


Fig. 4. Comparison of the RCS extracted from RC measurement using the two-step method and the simulated RCS obtained using CST Studio Suite in the -90° to $+90^\circ$ azimuth range in the VV polarization.

in regard to $\theta = 0^\circ$ as expected. This estimated distance gives the frequency of the sinusoidal signal whose amplitude is estimated by regression. The RCS is thus extracted by regression over a 0.9 GHz bandwidth according to the method detailed before.

The RCS pattern is shown in Fig. 4. We first of all notice it is close to being symmetrical with respect to $\theta = 0^\circ$. The comparison with simulation results shows the azimuth positions of the minima and maxima are in good agreement, and the close RCS values are obtained over both angular ranges $[-70^\circ; -10^\circ]$ and $[+10^\circ; +70^\circ]$. The highest difference between simulation and measurement is obtained around $\theta = 0^\circ$, but this difference stays below 2 dBm^2 on the whole azimuth range. This difference could be partly explained by the measurement setup. Indeed, the distance between the antennas and the target is slightly smaller than the far field distance; besides, a small angular gap is possible and could explain a part of the difference in the local minima.

C. HH Polarisation

Then, measurements are performed in the HH polarization and the RCS is extracted using the two-step method. So first, the distance is estimated over the 4 GHz frequency bandwidth

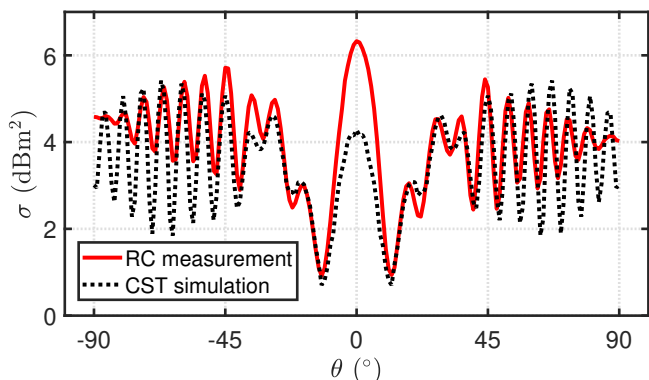


Fig. 5. Comparison of RCS extracted from RC measurement using the two-step method and RCS obtained from CST Studio Suite simulation in the -90° to $+90^\circ$ azimuth range in the HH polarization.

(red curve in Fig.3). The shallow excavation is visible on the distance estimation between θ between -14° and $+14^\circ$. This is consistent with the results in the VV polarization.

Then, the amplitude of the sinusoidal signal is estimated on the 0.9 GHz frequency bandwidth to retrieve the RCS value. The obtained RCS pattern is shown in Fig. 5 along with simulation results. Similar shapes are obtained with a good estimation of the maxima and minima locations. As in the VV measurement, the measurement and the simulation are in a good agreement between $[-50^\circ; -10^\circ]$ and $[+10^\circ; +50^\circ]$. The highest difference is for $\theta = 0^\circ$, but on the whole azimuth range the difference between both curves stays below 2 dBm^2 . As the RCS measured in the VV polarization, the RCS pattern in the HH polarization is symmetric with respect to $\theta = 0^\circ$.

V. CONCLUSION

This article deals with the demonstration that RCS measurement in RC could be a good alternative to the measurement in AC even for a complex target. The differential measurement (with and without target) and the two-step post-processing method permit to estimate the RCS pattern of an object with a satisfying accuracy. The antenna-target distance estimation is shown to lead with a remarkable accuracy to the position of the main scattered point. The RCS estimated though a regression process follows the simulated pattern obtained using the CST Studio Suite.

In this paper, a point-like target has been considered and the accuracy and the reliability of the proposed method has been demonstrated in this case. Further works will deal with more complex targets like multiple point scatterers or resonating targets that could require developing other signal processing approaches.

ACKNOWLEDGMENT

This work is supported by AID/DGA, France. It is also supported in part by the European Union through the European Regional Development Fund, in part by the Ministry of Higher Education and Research, in part by the Région Bretagne, and in part by the Département d'Ille et Vilaine through the CPER Project SOPHIE/STIC & Ondes.

- [1] P. Corona, G. Latmiral, E. Paolini, and L. Piccioli, "Use of a reverberating enclosure for measurements of radiated power in the microwave range," *IEEE Transactions on Electromagnetic Compatibility*, vol. EMC-18, no. 2, pp. 54–59, 1976.
- [2] P. Besnier and B. Démoulin, *Electromagnetic Reverberation Chambers*. ISTE Wiley & Sons, 08 2011.
- [3] G. Andrieu, "Electromagnetic Reverberation Chambers : Recent advances and innovative applications". The Institution of Engineering and Technology, 02 2021.
- [4] M. García-Fernández, D. Carsenat, and C. Decroze, "Antenna radiation pattern measurements in reverberation chamber using plane wave decomposition," *IEEE Transactions on Antennas and Propagation*, vol. 61, no. 10, pp. 5000–5007, 2013.
- [5] C. Lemoine, E. Amador, and P. Besnier, "On the k -factor estimation for rician channel simulated in reverberation chamber," *IEEE Transactions on Antennas and Propagation*, vol. 59, no. 3, pp. 1003–1012, 2011.
- [6] K. A. Remley, J. Dortmans, C. Weldon, R. D. Horansky, T. B. Meurs, C. Wang, D. F. Williams, C. L. Holloway, and P. F. Wilson, "Configuring and verifying reverberation chambers for testing cellular wireless devices," *IEEE Transactions on Electromagnetic Compatibility*, vol. 58, no. 3, pp. 661–672, 2016.
- [7] A. Soltane, G. Andrieu, and A. Reineix, "Monostatic radar cross-section estimation of canonical targets in reverberating room using time-gating technique," in *2018 International Symposium on Electromagnetic Compatibility (EMC EUROPE)*, 2018, pp. 355–359.
- [8] A. Sorrentino, G. Ferrara, M. Migliaccio, and S. Cappa, "Measurements of backscattering from a dihedral corner in a reverberating chamber," *Applied Computational Electromagnetics Society Newsletter*, vol. 33, pp. 91–94, 01 2018.
- [9] M. A. García-Fernández, D. Carsenat, and C. Decroze, "Antenna gain and radiation pattern measurements in reverberation chamber using doppler effect," *IEEE Transactions on Antennas and Propagation*, vol. 62, no. 10, pp. 5389–5394, 2014.
- [10] P. Besnier, J. Sol, and S. Méric, "Estimating radar cross-section of canonical targets in reverberation chamber," in *2017 International Symposium on Electromagnetic Compatibility - EMC EUROPE*, 2017, pp. 1–5.
- [11] A. Reis, F. Sarrazin, E. Richalot, S. Méric, J. Sol, P. Pouliguen, and P. Besnier, "Radar cross-section pattern measurements in a mode-stirred reverberation chamber: Theory and experiments," *IEEE Transactions on Antennas and Propagation*, pp. 1–1, 2021.
- [12] C. Charlo, P. Besnier, and S. Méric, "Quasi-monostatic radar cross-section measurement in reverberation chamber," in *2021 18th European Radar Conference (EuRAD)*, 2022, pp. 94–97.
- [13] C. Charlo, S. Méric, F. Sarrazin, E. Richalot, J. Sol, and P. Besnier, "Advanced analysis of radar cross-section measurements in reverberation environment," 2023. [Online]. Available: <https://arxiv.org/abs/2303.08751>